Locking of three coupled lasers

Hartmut Erzgräber[a], Sebastian Wieczorek[a], and Bernd Krauskopf[b]

[a] School of Engineering, Mathematics and Physical Sciences University of Exeter, Exeter EX4 4QF, United Kingdom
[b] Department of Engineering Mathematics, University of Bristol, Bristol BS8 1TR, United Kingdom

ABSTRACT

We investigate the stability of an array of three laterally coupled semiconductor lasers. This study of the simplest system with an underlying structure that is also found in larger arrays constitutes a first step towards understanding the stability properties of large arrays. We use a composite-cavity model, where the individual lasers are described by the transverse modes of the entire composite-cavity system. Specifically, we analyze the stable locking region, where the laser array exhibits continuous wave emission for different detunings and coupling strengths between the individual lasers. We find that the optical fields in the outer lasers are out of phase with the middle laser.

Keywords: composite-cavity model, coupled lasers, dynamics and bifurcations, numerical continuation

1. INTRODUCTION

Arrays of coupled semiconductor lasers have emerged as promising devices for high-power coherent light generation and already find many applications. However, a major difficulty in many applications is the sensibility of semiconductor lasers to external perturbations, such as coupling to another laser, which can lead to instabilities and chaotic dynamics [1–4]. Therefore, a better understanding of the coupling conditions for which a laser array is stable, that is, exhibits continuous wave emission, is very desirable.

In this paper we investigate the emission dynamics of three side-to-side coupled semiconductor lasers in a linear array as depicted in Figure 1. This forms the simplest system with an underlying structure that is also found in larger arrays. Namely, the laser in the middle is coupled to the two outer laser to the left and to the right. Hence, this study constitutes a first step towards understanding the stability properties of large arrays. More specifically, the laser array consists of three active regions that are separated by passive regions. The active sections are coupled via the evanescent optical field in the transversal x-direction. Laser emission takes place in the longitudinal z-direction. Here we restrict our study to the case where the two outer lasers are identical, $w_0 = w_A = w_C$, $n_A = n_B = 3.61$, and the distances between the two outer lasers and the middle laser are the same, $d = d_{AB} = d_{BC}$. The spatio-temporal dynamics of the electric field of this coupled laser array is governed by the inhomogeneous wave equation,

$$-\nabla^2\mathcal{E}(\vec{r},t) + \mu_0\sigma\frac{\partial\mathcal{E}(\vec{r},t)}{\partial t} + \mu_0\epsilon_0 n^2(\vec{r})\frac{\partial^2\mathcal{E}(\vec{r},t)}{\partial^2 t} = -\mu_0\frac{\partial^2\mathcal{P}(\vec{r},t)}{\partial^2 t}\,, \tag{1}$$

where $\mathcal{E}(\vec{r},t)$ is the electric field in the laser and $\mathcal{P}(\vec{r},t)$ is the macroscopic polarization. The function $n(\vec{r})$ takes into account the spatial variations of the refractive index. In semiclassical laser theory different concepts for obtaining (approximate) solutions to the wave equation have been developed. They include low-dimensional rate equations, which are ordinary differential equations [5–13], rate equations with time-delayed coupling [14–16], composite-cavity models [17–20], supermode models [21], and partial differential equation models including traveling-wave models [22–26]. Because of their simplicity, low-dimensional rate equation models are an attractive choice for the analysis of the stability and nonlinear dynamical behaviour with tools from bifurcation theory. However, these models neglect coupling effects in the space dependence of the electric field and are unsuitable for describing strongly coupled lasers. Partial differential equation models, on the other hand, are potentially very accurate but, due to their infinite-dimensional nature, they do not lend themselves easily to (comprehensive and global) stability analysis. The composite-cavity models strike a good compromise between

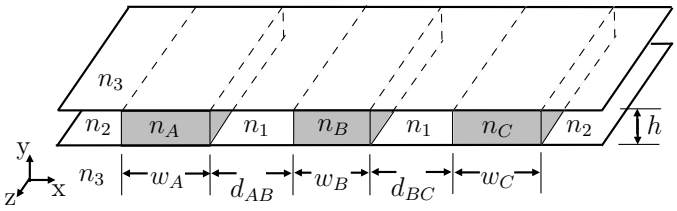

Figure 1. Sketch of the side-to-side coupled laser array, where $n_{A,B,C}$ are the refractive indices of lasers A,B, and C respectively. The lasers are separated by a passive section with refractive index n_1, and surrounded by cladding layers with refractive indices n_2 and n_3, respectively.

accuracy and suitability for bifurcation analysis. Most importantly, the stability and dynamics of this type of model can still be analysed with numerical continuation techniques [27].

This paper investigates a composite-cavity mode approach to modelling the general setup of an array of laterally coupled laser as shown in Figure 1. Namely, the individual stripes are coupled by the transverse modes of the entire composite-cavity system. Within the framework of semiclassical laser theory, we decompose the spatio-temporal dynamics of the laser array into time dependent complex-valued electrical field amplitudes and space dependent composite-cavity modes profiles [17, 18]. In particular, the coupling between the different stripes is included intrinsically in the composite-cavity mode structure, which makes this approach valid for arbitrary coupling. We perform a bifurcation analysis of composite-cavity modes for different geometries and refractive indices of laser stripes. Such a comprehensive analysis identifies the spatio-temporal dynamics of the composite-cavity modes. In particular, we find that for increasing values of the α-parameter stable continuous wave emission moves to lower laser coupling strength. In semiconductor lasers the α-parameter quantifies the refractive index effect in the laser [28].

This paper is structured as follows. In Section 2 we describe the composite-cavity approach. Moreover, we study the spatial profiles of the composite-cavity modes, their frequency as well as their gain and coupling coefficients as a function of the laser geometry. The composite-cavity mode structure is of great importance for the understanding the dynamics of the coupled laser array. This is discussed in Section 3, where we calculate the region of stable continuous wave emission in the parameter plane of laser distance d, which affects the laser coupling strength, and the α-parameter, which describes the amplitude-phase-coupling of the optical field. We finish with conclusions in Section 4.

2. COMPOSITE-CAVITY MODEL

We consider a laser device consisting of three laser stripes $\{A, B, C\}$ oriented along the longitudinal z-direction in which the laser beam is propagating, and coupled in the lateral x-direction as depicted in Figure 1. To analyse spatio-temporal instabilities in the laser array we decompose the total electric field in terms of spatial composite-cavity mode profiles $X_j(x)$ of the entire array [18, 29],

$$\mathcal{E}(x,t) = \frac{1}{2}\sum_j E_j(t)X_j(x) + c.c.\,, \tag{2}$$

where the $E_j(t)$ are the complex-valued time-dependent field amplitudes. Following Refs. [30–32] we focus on the x-direction only. Hence, the composite-cavity mode profiles $X_j(x)$ are solutions of the Helmholtz equation,

$$\left[\frac{\partial^2 X}{\partial x^2} + n^2(x)\frac{\Omega_j^2}{c^2} - k_z^2\right] X(x) \quad = 0\,, \tag{3}$$

together with appropriate boundary conditions [30, 31]. Here, $k_z = 5\pi \times 10^6$ m^{-1} is the z-component of the total wavevector, Ω_j is the composite-cavity mode frequency, and $n(x)$ reflects the refractive index variation in

the x-direction. In particular, we assume

$$n(x) = \begin{cases} n_g = 3.6 & \text{in the passive gaps between lasers,} \\ n_s = 3.61 & \text{in the active laser sections.} \end{cases}$$

The boundary conditions require that the electric field and its first derivative are continuous at each refractive index step and that they vanish at infinity. As in Ref. [31] we use sine functions in the active section and exponential functions in the passive section. Such solutions of the Helmholtz equation (3) satisfy the orthogonality relation

$$\int_{-\infty}^{\infty} n^2(x) X_j(x) X_{j'}(x) dx = \delta_{jj'} \mathcal{N} \,, \tag{4}$$

where $\delta_{jj'}$ is the Kronecker delta and $\mathcal{N} = \frac{n_b^2}{2}(3w_0 + 2d_0)$ is a normalization constant with $n_b = 3.6$, $w_0 = 4\mu$m, and $d_0 = 4\mu$m.

The time evolutions of the complex-valued electric field amplitude $E_j(t)$ associated with the composite-cavity mode $X_j(x)$ and the carrier density $N_s(t)$ in laser stripe s are governed by [17, 31]:

$$\begin{aligned} \frac{dE_j}{dt} =& -i(\Omega_j - \nu_j)E_j - \gamma E_j + \gamma \sum_{j'} \left\{ \sum_s K^s_{jj'} \left[(1 + \beta N_s) - i\alpha\beta(1 + N_s) \right] \right\} E_{j'} \,, \\ \frac{dN_s}{dt} =& \Lambda - (N_s + 1) - \sum_{j,j'} K^s_{jj'} (1 + \beta N_s) \mathrm{Re}[E_j E^*_{j'}] \,. \end{aligned} \tag{5}$$

Here the index $j = \{1, 2, 3\}$ refers to the three composite-cavity modes that are considered [Figure 2], $s = \{A, B, C\}$ refers to the three lasers, and the star denotes complex conjugation; see Ref. [18, 31] for details of the derivation. Most importantly, coupling between lasers occurs via the evanescent electric field in the lateral x-direction and depends on the laser distance d (or the width of the passive gap between the lasers) and the laser-width mismatch in the x-direction $\Delta = w_B - w_0$. Note that Eqs. (5) depend on the coupling parameters d and Δ implicitly via composite-mode frequencies Ω_j and the mode overlap integrals

$$K^s_{jj'} = \frac{n_s}{\mathcal{N}} \int_s X_j(x) X_{j'}(x) dx \tag{6}$$

over the respective active region s. We use typical semiconductor laser parameters that can be found in Table 1. These parameters give the normalised parameters in Eqs. (5) as decay rate $\gamma = 100$ and gain coefficient $\beta \approx 5.2$. Each laser is pumped at four times threshold, that is, $\Lambda = 4$. See also Ref. [31, 33] for the normalization of Eqs. (5).

Here, we define *locking* as a single-frequency solution of Eqs. (5), which is of the form

$$E_j(t) = |E^0_j| e^{-i(\omega^0 t + \varphi^0_j)} \,, \qquad N_s(t) = N^0_s \,, \tag{7}$$

where all nonzero complex-valued modal amplitudes have constant intensities $I_j = |E^0_j|^2$, the same optical frequency ω^0, a constant phase-shift φ^0_j, and each laser has a constant carrier density N^0_s. This describes

symbol	meaning	value
α	linewidth enhancement factor	$0 \leq \alpha \leq 2$
γ_E	cavity decay rate	$2 \times 10^{11} s^{-1}$
γ_N	carrier decay rate	$1 \times 10^{9} s^{-1}$
ξ	differential gain	$2.5 \times 10^{-20} m^2$
Γ	confinement factor	0.1
N_{ts}	carrier density at transparency	$2.0 \times 10^{24} m^{-3}$
n_b	background refractive index	3.6

Table 1. Laser parameters and their values.

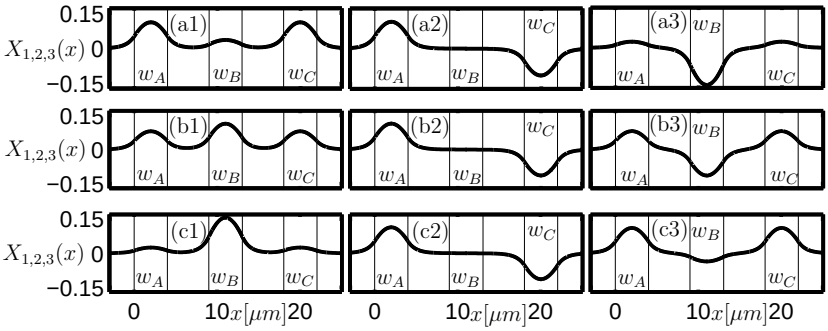

Figure 2. Spatial mode profiles $X_{1,2,3}(x)$ of the side-to-side coupled laser array for three different lateral width differences, (a): $\Delta = -0.05\mu m$, (b): $\Delta = 0\,\mu m$, (c): $\Delta = 0.05\,\mu m$

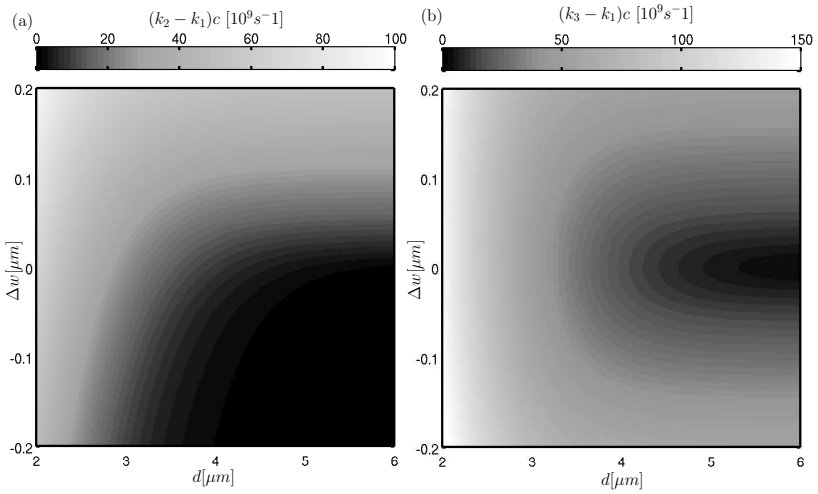

Figure 3. Composite-cavity mode detunings between mode 2 and mode 1 (a), and between mode 3 and mode 1 (b), as a function of the lateral width differences Δ and the laser distance d.

continuous wave emission of the coupled laser array. Simultaneous numerical continuation [27] of the composite-cavity mode profiles $X_j(x)$ and the locking solutions (7) unveils the stability diagram in the parameter plane of the laser distances and the width differences of the active laser sections.

Figure 2 shows examples of the spatial profiles $X_j(x)$ of the three composite-cavity modes ($j = 1, 2, 3$) that are considered here to model the dynamics of the laser array. There are two symmetrical modes ($j = 1, 3$) and one anti-symmetrical mode ($j = 2$). Figure 2 (a1)-(a3) shows the case $\Delta = -0.05$, where the two outer lasers are wider than the middle laser, Figure 2 (b1)-(b3) the case $\Delta = 0$, where all lasers are identical, and Figure 2 (c1)-(c3) the case $\Delta = 0.05$, where the middle laser is wider than the two outer lasers. As can be seen from Figure 2, changing Δ affects mainly modes 1, and 3. This is because these modes have a large amplitude in the middle laser. In contrast, mode 2 is almost unaffected by changes in Δ, because this mode is almost zero in the middle laser.

To further unveil the composite-cavity mode structure we now calculate the frequency Ω_j and the overlap integrals $K^s_{jj'}$. Figure 3 shows the detunings between the composite-cavity modes as a function of the distance d between the laser and the laser width difference Δ. Figure 3(a) shows the detuning $(k_2 - k_1)c$ between mode 1 and mode 2. The detuning is small for large d and sufficient negative Δ. Figure 3(b) shows the detuning $(k_3 - k_1)c$ between mode 1 and mode 3. The detuning is small for large d around $\Delta = 0$.

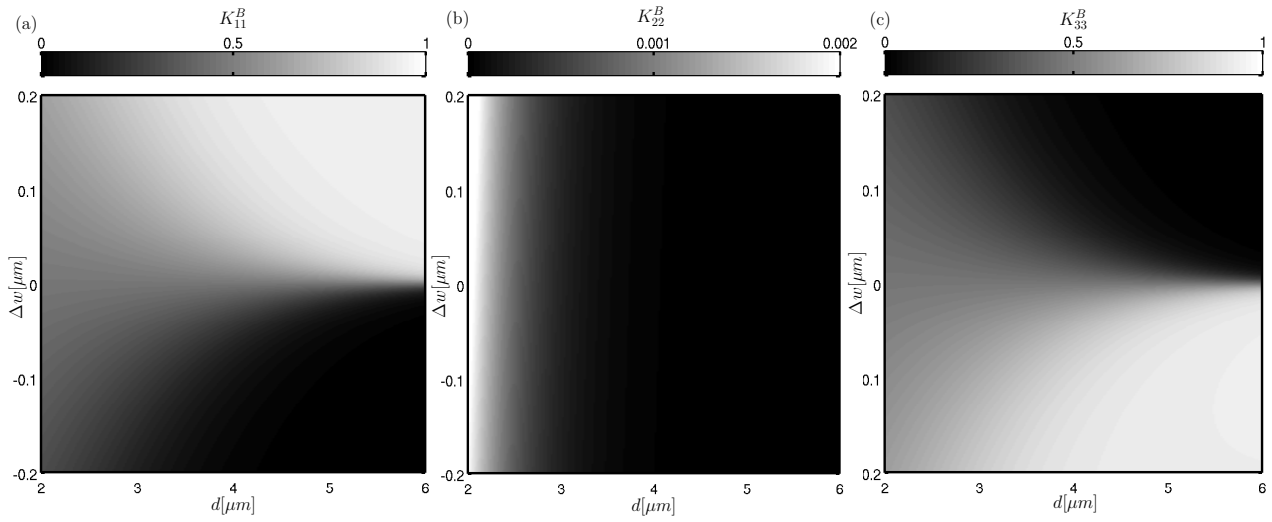

Figure 4. Composite-cavity mode gains K_{jj}^B of mode ($j = 1$) (a), mode ($j = 2$) (b), and mode ($j = 3$) (c) in cavity B, as a function of the lateral width differences Δ and the laser distance d.

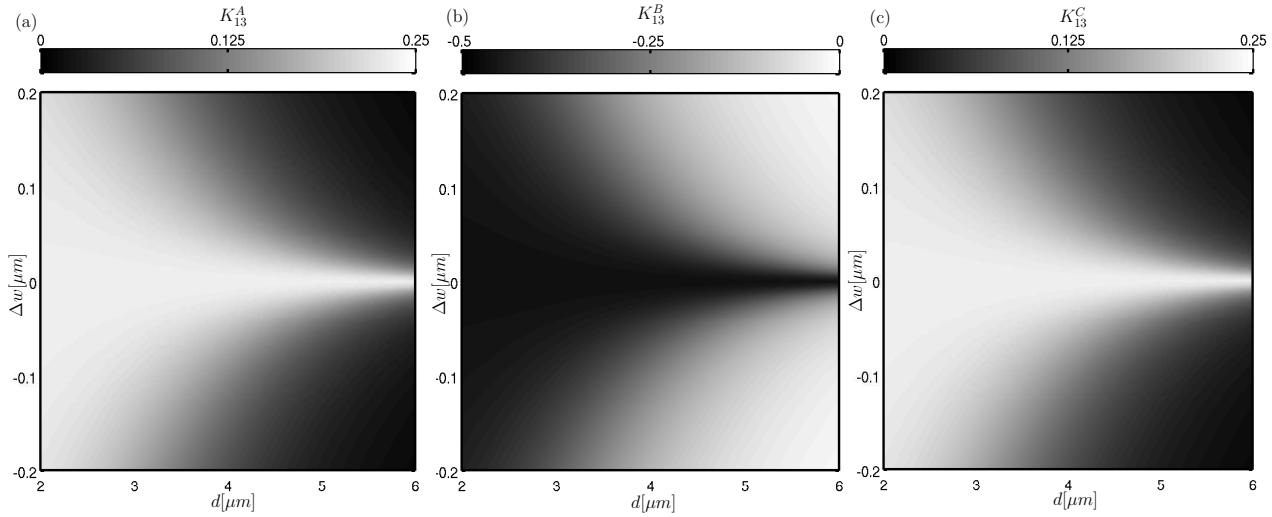

Figure 5. Composite-cavity mode coupling K_{13}^s between mode 1 and mode 3 in cavity ($s = A$) (a), cavity ($s = B$) (b), and cavity ($s = C$) (c), as a function of the lateral width differences Δ and the laser distance d.

Finally, Figures 4 and 5 show examples of the gain and coupling coefficients $K_{jj'}^s$ as a function of the laser distance d and the laser width difference Δ. In particular, Figure 4 shows the modal gains K_{jj}^B in laser B. The variations of both K_{11}^B [Figure 4 (a)] for mode 1 and K_{33}^B [Figure 4 (c)] for mode 1 are large. For sufficient large distance d, the gain coefficient of mode 1 increases form 0 for $\Delta < 0$ to 1 for $\Delta > 0$. The gain coefficient of mode 3 shows the opposite behavior. As the distance d gets smaller, these gain coefficients approach 1/3, which indicates that these modes have comparable amplitudes in all three laser; also compare with Figure 2. In contrast, the gain coefficient K_{22}^B [Figure 4 (b)] of mode 2 is almost 0 in laser B and shows only little variations as d or Δ are changed. Indeed, comparison with Figure 2 shows that mode 2 is almost zero in laser B.

Coupling between modes arises from their spatial overlap with the different lasers. Two modes are coupled

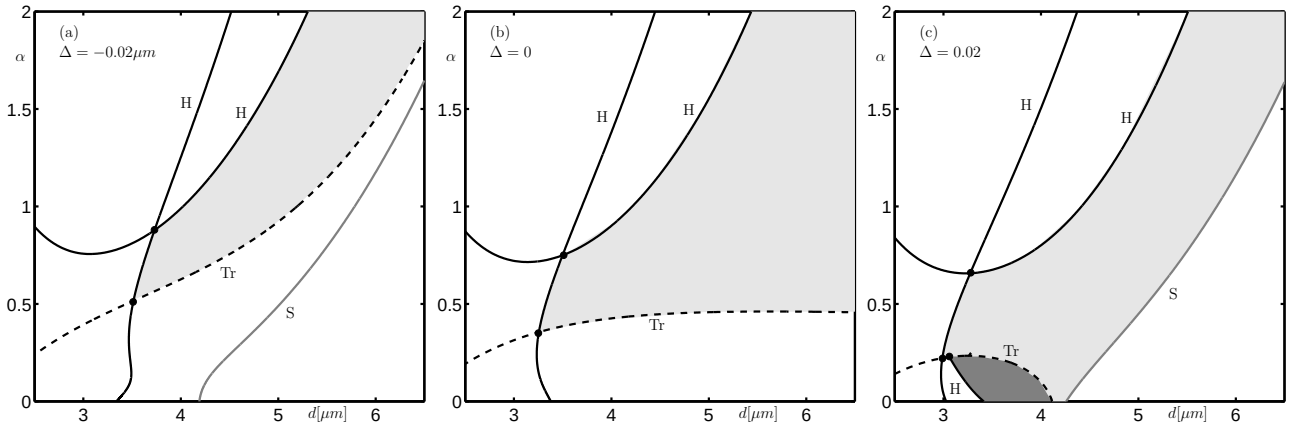

Figure 6. Bifurcation diagram of the side-to-side coupled laser array as a function of the laser distance d and the linewidth enhancement factor α, for different values of Δ as indicated. Shown are curves are Hopf (H), saddle-node (S), and transcritical (Tr) bifurcations; the locking region is shaded gray, where lighter shading indicates locking with mode 1 and 3 having nonzero intensity, and darker shading indicates locking with nonzero intensity of all three modes.

only if both have nonzero amplitude in lasers A,B,C. Hence, coupling coefficients involving mode 2 in laser B are very small and insensitive to changes in d and Δ. Moreover all coupling coefficients exhibit almost symmetrical behavior about the line $\Delta = 0$. Figure 5 shows the coupling coefficients between mode 1 and mode 3 in the three different lasers A,B,C. Both mode 1 and mode 3 have positive amplitude in lasers A and C. Their coupling coefficients K_{13}^A [Figure 5 (a)] and K_{13}^C [Figure 5 (c)] exhibit similar behavior. In contrast mode 1 and mode 3 have opposite amplitudes in lasers B. Hence, the coupling coefficient K_{13}^B is negative [Figure 5 (b)].

3. COMPOSITE-CAVITY MODE DYNAMICS

In the previous section we discussed the frequency and the spatial properties of the composite-cavity modes, which are the solution of the Helmholtz equation (3) together with the boundary conditions arising from Eq. (4).

To reveal the bifurcation structure and the dynamics of the coupled laser array we use numerical continuation with AUTO [27]. Here we concentrate on the influence of the amplitude-phase-coupling of the optical field, which is quantified by the α-parameter, as well as on the influence of the distance d between the laser, which affects the coupling strength between the lasers. We calculate locking regions where the laser array exhibits stable continuous wave (cw) emission described by Eq. (7). The boundaries of these locking regions are formed by different bifurcation curves, including Hopf (H), saddle-node (S), and transcritical (Tr) bifurcations.

Figure 6 shows the locking regions in the parameter plane of laser distance d and linewidth enhancement factor α for three different values of the laser width difference Δ. The locking region is indicated by gray shading. The light gray regions indicate locking where only composite-cavity mode 1 and 3 have nonzero intensity $|E_{1,3}^0|^2 \neq 0$ and mode 2 has zero intensity $|E_2^0|^2 = 0$. In contrast, the dark gray region indicates locking where all three composite-cavity modes have nonzero intensity $|E_{1,2,3}^0|^2 \neq 0$.

Figure 6(a) shows the case for $\Delta = -0.02\mu m$, where the two outer lasers are wider than the middle laser. In particular, it can be seen that there is no stable cw-emission for small α-parameter, namely for $\alpha < 0.5$. For sufficient large α the locking region is bounded by Hopf (H) and transcritical (Tr) bifurcation curves. When crossing the Hopf (H) bifurcation curve the cw-emission looses stability and exhibits periodic oscillations of the intensity. When crossing the transcritical (Tr) bifurcation curve the cw-emission looses stability because mode 2 crosses its threshold and gains nonzero intensity. However, the resulting three-mode locked state is not stable. Moreover, it can be seen that the locking region moves to larger d, that is, weaker laser coupling strength, as the α-parameter is increased. Figure 6(b) shows the case when all laser are identical $\Delta = 0$. Also in this case there is no stable cw-emission for small values of the α-parameter, namely for $\alpha < 0.3$. The locking region is bounded

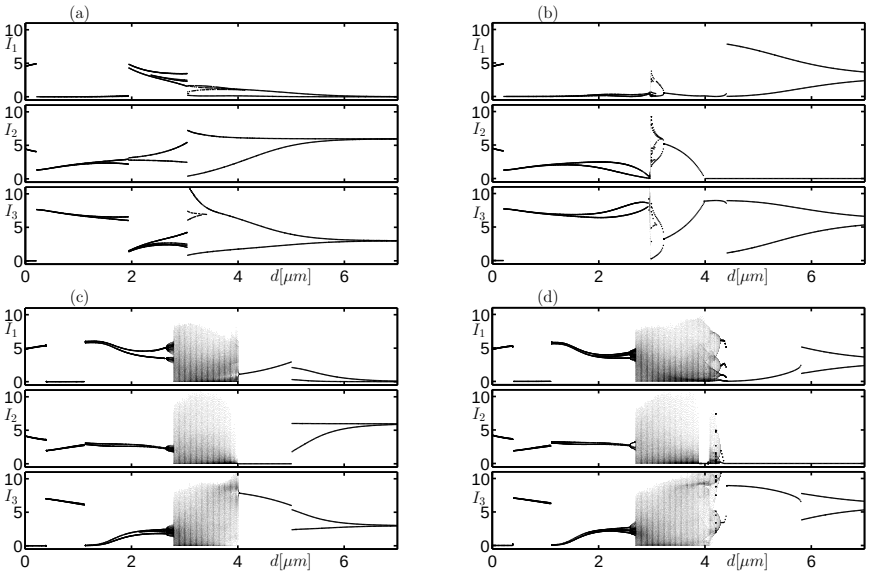

Figure 7. The modal intensities as a function of the laser distance d for two different the lateral width differences Δ and two different values of the linewidth enhancement factor α. Panels (a): $\alpha = 0, \Delta = -0.02$, panels (b): $\alpha = 0, \Delta = 0.02$, panels (c): $\alpha = 1, \Delta = -0.02$, panels (d): $\alpha = 1, \Delta = 0.02$.

by Hopf (H) bifurcation curves toward decreasing d, that is, increasing laser coupling strength. Since all lasers are identical, the locking region extends to arbitrary weak coupling. Finally, Figure 6(c) shows the case for $\Delta = 0.02\,\mu m$, where the middle lasers is wider than the two outer lasers. In contrast to the previous case, there is stable cw-emission where all three modes have nonzero intensity, that is, $|E^0_{1,2,3}| \neq 0$ (dark gray region). Moreover, the locking region now also extends to $\alpha = 0$. When crossing the transcritical (Tr) bifurcation curve between the two-mode (light gray) and three-mode (dark gray) locking region, mode 2 crosses its threshold and gains nonzero intensity. In contrast to the previous cases, this state is now stable. For sufficiently large α the two-mode locking region is bounded by Hopf (H) curves toward decreasing d, and by a saddle-node (S) curve toward increasing d. Again, as in the case of $\Delta = 0.02\,\mu m$ [Figure 6 (a)], the locking region moves towards larger distances d, that is, weaker laser coupling strength, as the α-parameter is increased.

Because the different composite-cavity modes have different spatial profiles, different modal amplitudes $|E_j|$ result in different spatial intensity patterns of the coupled laser array. Figure 7 further reveals contributions of the different modes to the dynamics of the coupled laser array. Shown are one-parameter bifurcation diagrams, where we plot the extrema of the modal intensities $|E_j|^2$ as a function of the distance d for two different values of α and Δ. Specifically, Figure 7(a) shows the case $\alpha = 0$ and $\Delta = -0.02$. By increasing the distance between the lasers from $d = 0$ to $d = 6.5$ the coupled laser array exhibits different periodic intensity oscillation characterized by their minima and maxima. In particular, for very small and very large d these oscillations have very small amplitude. Figure 7(b) shows the case $\alpha = 0$ and $\Delta = 0.02$, where there is a stable two-mode cw-emission around $d = 4.5$ that is dominated by mode 3. This corresponds to the state where the electric field in the middle laser is out-of-phase with that of the two outer lasers; compare with Figure 2. At $d \approx 4$ there is a transcritical (Tr) bifurcation and mode 2 gains nonzero intensity. Now also the two outer lasers are out-of-phase to each other. For $\alpha = 1$ the dynamics of the laser array can be much more complicated as can be seen in Figures 7(c) and (d). In particular, there is a large region of chaotic dynamics around $d = 3$. For very large and very small d the laser array exhibits periodic intensity oscillations. Finally, there is a region of stable cw-emission around $d = 5$. The cw-emission is dominated by mode 3, which indicates out-of-phase oscillation of the electric field in the middle laser and the two outer lasers.

4. CONCLUSIONS

We investigated the dynamics of a laterally coupled semiconductor laser structure that consists of three lasers separated by passive sections. Our study was restricted to the case where the two outer laser are identical and the distances between the outer lasers and the middle laser are equal. This system was modeled in the composite-cavity approach, which describes the dynamics of the coupled laser array by three coupled composite-cavity modes. The variation of the mode frequency, the modal gain coefficients and the modal coupling coefficients due to changes of the laser geometry are accurately taken into account by calculating the composite-cavity mode profiles.

A bifurcation analysis of the composite-cavity mode model was performed to determine the dynamics of the laser array. In particular, we found different locking regions, where either two modes have nonzero intensity, or all three modes have nonzero intensity. Three-mode locking exists for sufficiently small values of the α-parameter. Moreover, we found that stable continuous wave emission moves toward weaker laser coupling as the α-parameter is increased.

Future research will study the three-laser system in dependence on other paramters, for example, when the symmetric situation considered here is perturbed. Furthermore, the composite-cavity approach can also be used to study the (locking) dynamics of more complicated laser arrays.

ACKNOWLEDGMENTS

This research was supported by Great Western Research Fellowship 18 "Modelling and nonlinear dynamics of optical nanodevices: nanolasers and photonic nanocircuits."

REFERENCES

1. C. Weiss and R. Vilaseca, *Dynamics of lasers*, VCH Publishing, 1991.
2. D. Botez and D. Scifres, eds., *Diode Laser Arrays*, Cambridge University Press, 1994.
3. W. Chow and S. Koch, *Semiconductor-Laser Fundamentals*, Springer-Verlag, Berlin, 1999.
4. B. Krauskopf and D. Lenstra, eds., *Fundamental Issues of Nonlinear Laser Dynamics*, vol. 548 of *AIP Conference Proceedings*, American Institute of Physics, 2000.
5. O. Hess and E. Schöll, "Spatio-temporal dynamics in twin-stripe semiconductor lasers," *Physica D: Nonlinear Phenomena* **70**, pp. 165–177, Jan. 1994.
6. O. Hess and E. Schöll, "Eigenmodes of the dynamically coupled twin-stripe semiconductor laser," *Phys. Rev. A* **50**, pp. 787–792, Jul 1994.
7. D. Merbach, O. Hess, H. Herzel, and E. Schöll, "Injection-induced bifurcations of transverse spatiotemporal patterns in semiconductor laser arrays," *Phys. Rev. E* **52**, pp. 1571–1578, Aug 1995.
8. P. De Jagher, M. Yousefi, and D. Lenstra, "A 2-oscillator model for the twin-stripe cavity," in *Proceedings of SPIE*, 2003.
9. J. R. Terry, K. S. Thornburg, D. J. DeShazer, G. D. VanWiggeren, S. Zhu, P. Ashwin, and R. Roy, "Synchronization of chaos in an array of three lasers," *Phys. Rev. E* **59**, pp. 4036–4043, Apr 1999.
10. P. Mandel, L. Ruo-ding, and T. Erneux, "Pulsating self-coupled lasers," *Phys. Rev. A* **39**, pp. 2502–2508, Mar 1989.
11. J. García-Ojalvo, T. M. C., and V. R., "Spatiotemporal dynamics of dressed broad-area lasers," *Quantum and Semiclassical Optics* **10**, pp. 809–821, 1998.
12. J. García-Ojalvo, M. Brambilla, M. C. Torrent, and R. Vilaseca, "Coupled transverse modes in three-level cascade lasers," *Chaos, Solitons and Fractals* **10**, pp. 819–824, 1999.
13. S. Yanchuk, A. Stefanski, T. Kapitaniak, and J. Wojewoda, "Dynamics of an array of mutually coupled semiconductor lasers," *Physical Review E (Statistical, Nonlinear, and Soft Matter Physics)* **73**(1), p. 016209, 2006.
14. J. Mulet, C. Mirasso, T. Heil, and I. Fischer, "Synchronization scenario of two distant mutually coupled semiconductor lasers," *J. Opt. B: Quantum Semiclass. Opt.* **6**, pp. 97–105, 2004.

15. J. Mulet, C. Masoller, and C. R. Mirasso, "Modeling bidirectionally coupled single-mode semiconductor lasers," *Phys. Rev. A* **65**, p. 063815, Jun 2002.
16. H. Erzgräber, D. Lenstra, B. Krauskopf, E. Wille, M. Peil, I. Fischer, and W. Elsäßer, "Mutually delay-coupled semiconductor lasers: Mode bifurcation scenarios," *Opt. Commun.* **255(4-6)**, pp. 286–296, 2005.
17. S. A. Shakir and W. W. Chow, "Semiclassical theory of coupled lasers," *Opt. Lett.* **9**(6), p. 202, 1984.
18. S. A. Shakir and W. W. Chow, "Semiclassical theory of coupled lasers," *Phys. Rev. A* **32**, pp. 983–991, Aug 1985.
19. W. W. Chow, "Frequency locking in an index-guided semiconductor laser array," *J. Opt. Soc. Am. B* **3**, pp. 833–836, 1986.
20. S. Wieczorek and W. W. Chow, "Bifurcations and interacting modes in coupled lasers: A strong-coupling theory," *Physical Review A (Atomic, Molecular, and Optical Physics)* **69**(3), p. 033811, 2004.
21. E. Kapon and J. Katz, "Supermode analysis of phase-locked arrays of semiconductor lasers," *Opt. Lett.* **9**(4), p. 125, 1984.
22. P. Ru, P. K. Jakobsen, J. V. Moloney, and R. A. Indik, "Generalized coupled-mode model for the multistripe index-guided laser arrays," *J. Opt. Soc. Am. B* **10**(3), pp. 507–515, 1993.
23. B. Krauskopf and D. Lenstra, eds., *Fundamental Issues of Nonlinear Laser Dynamics*, vol. 548 of *AIP Conference Proceedings*, ch. O. Hess, Theory and Simulation of Spatially Extended Semiconductor Lasers, pp. 128–148. American Institute of Physics, 2000.
24. C. R. Mirasso, M. Kolesik, M. Matus, J. K. White, and J. V. Moloney, "Synchronization and multimode dynamics of mutually coupled semiconductor lasers," *Phys. Rev. A* **65**, p. 013805, Dec 2001.
25. M. Matus, J. V. Moloney, and M. Kolesik, "Relevance of symmetry for the synchronization of chaotic optical systems and the related lang-kobayashi model limitations," *Phys. Rev. E* **67**, p. 016208, Jan 2003.
26. J. Piprek, ed., *Optoelectronic Devices - Advanced Simulation and Analysis*, ch. M. Radziunas and H. J. Wünsche, Multisection Lasers: Longitudinal Modes and their Dynamics. Springer, New York, 2004.
27. E. Doedel, A. Champneys, T. Fairgrieve, Y. Kuznetsov, B. Oldeman, R. Paffenroth, B. Sandstede, X. Wang, and C. Zhang, "AUTO-07P: continuation and bifurcation software for ordinary differential equations," tech. rep., Concordia University, Montreal, Canada, 2007.
28. C. H. Henry, "Theory of the linewidth of semiconductor lasers," *IEEE J. Quantum Electron.* **18**, pp. 259–264, 1982.
29. W. W. Chow, "A compisite-resonator mode description of coupled lasers," *IEEE J. Quantum Electron.* **QE-22(8)**, pp. 1174–1183, 1986.
30. W. W. Chow, "Effects of spatial gain variation in an index-guided semiconductor laser array," *J. Opt. Soc. Am. B* **4**(3), p. 324, 1987.
31. H. Erzgräber, S. Wieczorek, and B. Krauskopf, "Dynamics of two laterally coupled semiconductor lasers: Strong- and weak-coupling theory," *Physical Review E* **78**(6), p. 066201, 2008.
32. H. Erzgräber, S. Wieczorek, and B. Krauskopf, "Locking behavior of three coupled laser oscillators," *Physical Review E* **80**(2), p. 026212, 2009.
33. S. Wieczorek and W. W. Chow, "Global view of nonlinear dynamics in coupled-cavity lasers — a bifurcation study," *Optics Communications* **246**, pp. 471–493, Feb. 2005.